INSTITUTE OF PHYSICS PUBLISHING JOURNAL OF PHYSICS D: APPLIED PHYSICS

J. Phys. D: Appl. Phys. **37** (2004) 638–643 PII: S0022-3727(04)70363-0

Ablation of metals by ultrashort laser pulses

N N Nedialkov, S E Imamova and P A Atanasov

Institute of Electronics, Bulgarian Academy of Sciences, 72, Tsarigradsko Shose, Sofia 1784, Bulgaria

E-mail: gaslaser@ie.bas.bg

Received 14 October 2003
Published 28 January 2004
Online at stacks.iop.org/JPhysD/37/638 (DOI: 10.1088/0022-3727/37/4/016)

Abstract

Ablation of Fe by ultrashort laser pulses with durations 0.1, 1, and 5 ps were investigated experimentally. The laser fluence varied from the ablation threshold up to 100 J cm^{-2}. Above 1 J cm^{-2}, the ablation rate depended on the laser pulse duration, with the shortest pulse producing the highest value. A change in the ablation rate as the laser fluence increased was also observed. These results were analysed using molecular dynamics simulations. We show that the change in the ablation rate is connected to an overheating of the material above the critical point, which results in a steep rise of the pressure developed. Furthermore, due to the electron heat diffusion, the overheated volume increases and involves material located deeper than the skin depth. An increase in the pulse duration results in a decrease in the degree of overheating.

1. Introduction

The growing application of laser systems generating ultrashort laser pulses in the field of material processing is based on the advantages that they offer compared with nanosecond pulses. Experiments on micro-machining of a wide range of materials by ultrashort pulses [1–4] have shown that they ensure negligible heat diffusion into the material and absence of plasma during the laser pulse. As a consequence, the ablation threshold decreases (by one order of magnitude in some cases [4]) compared with nanosecond pulses, so that precise sub-micron machining becomes possible with minimization of the heat affected zone. Indeed, application of ultrashort laser pulses proved to be particularly suitable for the treatment of materials having high heat conductivity, e.g. metals and semiconductors.

Recent studies [5–14] have shown that the process of interaction of ultrashort laser pulses with matter is very complicated and is strongly influenced by the parameters of the laser radiation, the properties of the material, the processing conditions, and the environment. Experimental works on laser ablation of metals [5–7] have indicated that, in contrast to the case with nanosecond pulses, the electron thermal diffusion can play an important role in the process of dissipation of the absorbed energy and the properties of the electron–phonon coupling are important for femtosecond laser induced damage. It has also been shown that the process of ablation can be accompanied by a fast nonlinear phase transition, such as melting and amorphization [11], and formation of three-dimensional structures within the ablation region [9, 10, 13] which affect the ablation rate. Drilling by high laser intensities (10^{15} W cm^{-2}) [15] has shown that some of the advantages of using ultrashort pulses can be lost. Laser ablation with such intensities is accompanied by a considerable amount of molten material and high temperature gradients, leading to stresses, which can cause deformations, dislocations, or crack formation in the material.

The presence of different processes in ultrashort laser ablation makes its theoretical modelling difficult. In addition, some of the processes involved are not clearly understood. However, some recent theoretical investigations [8, 15–17], based mostly on molecular dynamics simulations, two-temperature heat diffusion models, and fluid dynamics models, have shown that some of the main features of the process could be described and explained. It was demonstrated that the process of ejection of the material incorporates various mechanisms—spallation, phase explosion, fragmentation, and evaporation.

In the framework of MD simulations, the investigated materials are examined at a microscopic level as the interactions between particles and the dynamics of the different phases can be obtained without any considerations of the

character of the processes involved. In spite of the classical MD simulations having some limitations in terms of the size of the simulated system and the time for evolution tracing, they have been proved to give an adequate description of the main features of ultrashort pulses–material interactions.

In this paper, we present experimental results on ultrashort laser ablation of iron. In order to investigate the process at different processing conditions, the experiments were performed at three pulse durations, $\tau_p = 0.1$, 1, and 5 ps, and in a wide laser-fluence range—from the threshold up to 100 J cm^{-2}. The results obtained were analysed by molecular dynamics simulations.

2. Experimental set-up

The experiments were carried out using a Ti : sapphire laser system (Spectra Physics Hurricane, $\lambda = 800$ nm). The system is based on the chirped-pulse amplification technique, and continuous variation of the pulse duration from 0.1 to 6 ps is available. The pumping laser is Nd : YAG operating at the second harmonic and 1 kHz repetition rate. The desired number of pulses was controlled by a fast mechanical shutter. The laser fluence was determined by measuring the pulse energy and the spot size on the sample plane. A lens with 100 mm focal length was used to focus laser radiation. It produced a spot with a diameter of 18 μm on the sample. The fluctuation of the pulse energy from pulse to pulse was below 10%. The targets were 99.5% pure Fe plates with a thickness of 0.5 mm. The samples were placed in a vacuum chamber at a pressure of 1 mbar. The ablation depth per pulse was obtained by dividing the total depth of the hole produced by the number of pulses used. A laser scanning microscope (LSM) was used to observe the ablated area and to measure the ablation depth. The total depth of the hole was measured from the hole profile obtained by the LSM. The number of pulses used to produce a hole (or total depth) was determined by the sensitivity of the LSM; it varied from 1000 at the lowest fluence to ten at the highest one.

3. Modelling

The simulations were performed on the basis of the classical molecular dynamics technique [18]. The numerically stable and simple velocity Verlet algorithm was applied to integrate the equation of motion. The interaction between the atoms in the system was described by the Morse potential, with the parameters for Fe taken from [19]. This choice was made with the purpose of decreasing the computation time. Although this potential does not take into account many-body interactions, as potentials based on the embedded atom method do, it has been found to give a good description of the properties of the body-centred cubic metals and their liquid phase. A comparison of experimental data with the values of material parameters, such as elastic constants, evaluated on the basis of the Morse potential, gives a maximal deviation of 20%. This discrepancy is not significant, which is confirmed by the theoretical results obtained and a comparison with the experimental data, as described later.

In order to avoid interactions between atoms at distances longer than the potential cutoff radius, the calculations were organized using the cell structure and the link-list method [18].

The structure of the body-centred cubic Fe cell was used to define the initial positions of the atoms. The simulated system was constructed by a certain number of unit cells in the x-, y-, and z-directions. In order to save computational time, the size of the system was varied with the laser fluence. The number of atoms in the simulations varied from 30 000 at low fluences up to 100 000 at high fluences. The initial velocities were randomly ascribed to the atoms according to the Maxwell distribution at room temperature.

In order to simulate an infinite medium, periodic boundary conditions for the atoms were applied in the x- and y-directions of the computational domain. This means that the processes occurring at the centre of the laser spot were examined and the effects at the edges of the laser spot were neglected. A velocity dampening technique was applied at the bottom of the computational cell in order to eliminate the artificial ablation effects that arise from the shock-wave reflection from the bottom boundary of the system. In order to render a precise description of the processes related to the effects at the edges of the laser spot, the process was also studied in a second configuration. The laser pulse, having a Gaussian spatial intensity distribution, was focused on the surface of the simulation system.

We simulated the interaction of laser pulses with $\tau_p = 0.1$ and 5 ps and wavelength $\lambda = 800$ nm with Fe. The laser beam intensity was assumed to have a Gaussian temporal distribution. A number of photons, corresponding to the laser energy, were deposited in the material exponentially following the Lambert–Beer law. The energy of the photons was transferred to the atoms of the system within a characteristic time, τ_{eq}, corresponding to the time of electron–lattice energy transfer and establishment of the equilibrium temperature. The energy deposited to the atoms in the system contributes to an increase in their kinetic energy. The time, τ_{eq}, depends on the properties of the material and is of the order of several picoseconds and up to several tens of picoseconds in the case of metals [14, 17]. According to the two-temperature diffusion model [5–7],

$$\tau_{eq} \approx \frac{\tau_e \tau_p(\tau_p + \tau_i)}{\tau_e(\tau_p + \tau_i) + \tau_p \tau_i} + \frac{\tau_e \tau_i}{\tau_e + \tau_i}, \tag{1}$$

where $\tau_i = C_i/\gamma$ and $\tau_e = C_e/\gamma$, are the electron cooling and lattice heating times, respectively, C_i and C_e are the lattice and electron heat capacities, and γ is a parameter characterizing the electron–lattice coupling. The estimation yielded 5 ps for the case of $\tau_p = 0.1$ ps and 8.5 ps for $\tau_p = 5$ ps.

The model accounts for the electron thermal diffusion by increasing the effective depth of laser energy penetration. This depth was estimated from the electron thermal diffusion length:

$$l_{th}^{e} \approx (D_e \tau_{eq})^{1/2}, \tag{2}$$

where $D_e = K_e/C_e$ is the electron thermal diffusion coefficient. The electron thermal conductivity, K_e, and the electron heat capacity, C_e, were obtained using the relations

$$C_e = A_e T_e, \qquad K_e = \alpha\theta_e \frac{(\theta_e^2 + 0.16)^{5/4}(\theta_e^2 + 0.44)}{(\theta_e^2 + 0.092)^{1/2}(\theta_e^2 + \beta\theta_i)},$$

$$\theta_e = \frac{T_e}{T_F}, \qquad \theta_i = \frac{T_i}{T_F},$$

Table 1. Fe parameters used in the calculations.

A_e ($J\,m^{-3}\,K^{-2}$)	α ($W\,m^{-1}\,K^{-1}$)	β	E_F (eV)	γ ($W\,m^{-3}\,K^{-1}$)	C_i ($J\,m^{-3}\,K^{-1}$)	R (%)
67.2	116	1.2	7.3	3×10^{17}	3.8×10^{6}	65

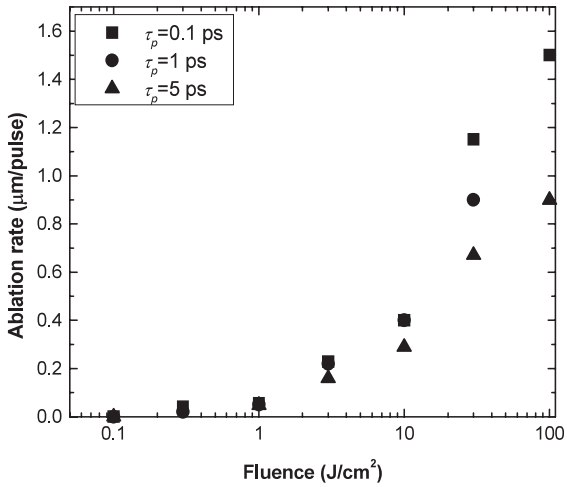

Figure 1. Dependence of the ablation rate (depth per pulse) on the laser fluence at $\tau_p = 0.1$, 1, and 5 ps for Fe.

where T_e and T_i are the electron and lattice temperatures and T_F is the temperature corresponding to the Fermi energy, E_F [5–7, 16]. The temperatures T_e and T_i were estimated from an analytical solution of the two-temperature diffusion model [1, 5–7]. The Fe parameters [5–7, 16, 20–22] used in the calculations are given in table 1. Due to the limitations of the MD modelling in terms of the number of particles, in the case of the Gaussian spatial intensity distribution, the laser pulse was focused on an area of several nanometers squared and the depth, $1/\alpha$ (α being the absorption coefficient), and the electron thermal diffusion length were reduced by a factor of 20. The energy deposited was estimated from the volume density of photons corresponding to the real conditions and scaled for our volume.

4. Results and discussions

The dependence of the ablation rate (depth per pulse) on the laser fluence for Fe is shown in figure 1. The experimental data presented are for the three pulse durations—0.1, 1, and 5 ps. Regardless of the laser pulse duration, one can define different ablation modes: at low laser fluences (up to $\sim 1\,J\,cm^{-2}$), the ablation rate increases slowly with the laser fluence and small variations are only seen in the ablation depths for the different pulse durations, while the increase in the laser fluence results in a steep rise in the ablation depth and in different ablation rates for the different pulse durations, with the shortest laser pulse producing the highest ablation rate.

The different ablation modes occurring at low and high laser fluences are characterized by different features of the ablated region and affect the holes drilled in the materials. Figure 2 presents LSM images of the ablated holes at a pulse duration of 0.1 ps and laser fluences $F = 0.3$ and $10\,J\,cm^{-2}$. The bottom of the drilled hole has a rough surface and presence

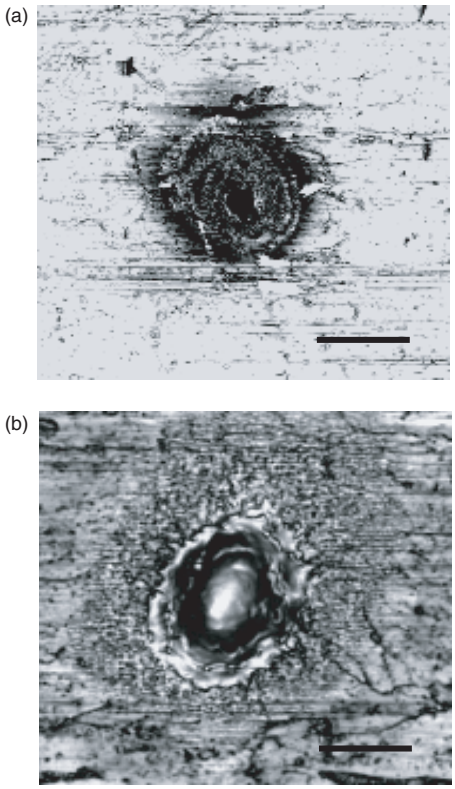

Figure 2. LSM images of holes ablated in Fe at $\tau_p = 0.1$ ps for (*a*) $F = 0.3\,J\,cm^{-2}$, 100 pulses; (*b*) $F = 10\,J\,cm^{-2}$, 10 pulses. The black mark in each image has a length of 15 μm.

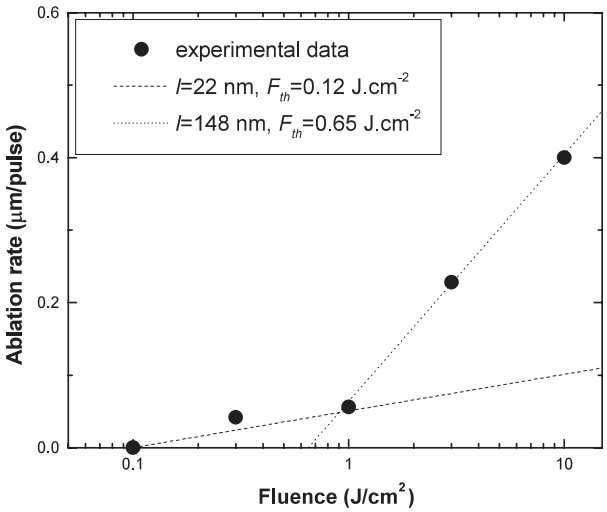

Figure 3. Ablation rate in Fe as a function of the laser fluence at $\tau_p = 0.1$ ps. The lines represent results obtained by equation (3) at the different values of l and F_{th} given in the inset.

of the molten phase is not evident at the low fluence. However, a trace of molten material that has solidified around the hole is clearly seen at higher laser fluences.

The existence of the second ablation rate is often [5, 7] explained by the contribution of the electron thermal diffusion to the dissipation of the absorbed energy. Figure 3 presents experimental results for the ablation rate in Fe as a function of the laser fluence for a laser pulse duration of $\tau_p = 0.1$ ps.

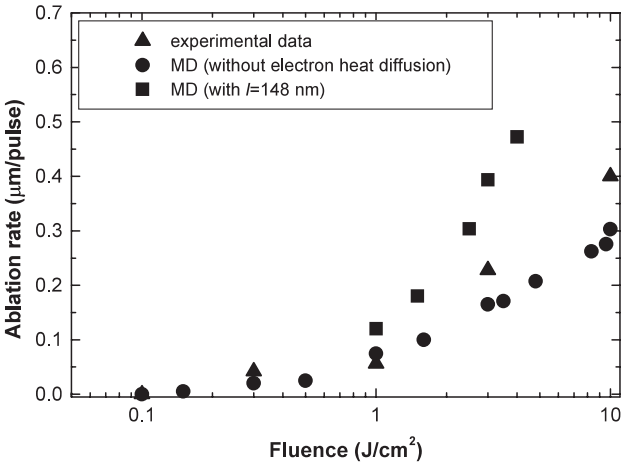

Figure 4. Ablation rate in Fe as a function of the laser fluence at $\tau_p = 0.1$ ps for different conditions of electron heat diffusion.

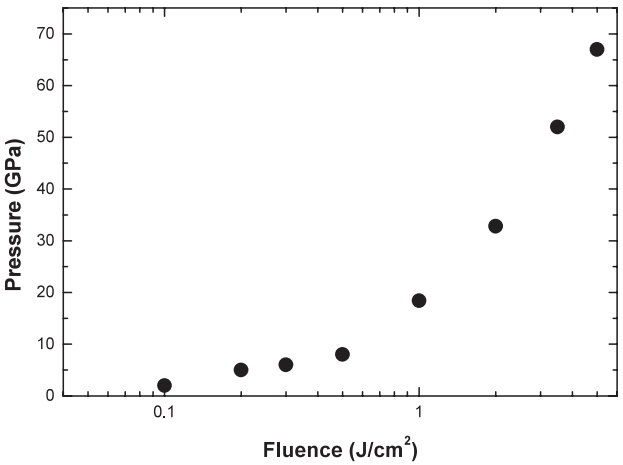

Figure 5. Dependence of the maximal pressure developed in the absorbing volume on the laser fluence at $\tau_p = 0.1$ ps.

The lines in figure 3 depict the relation

$$D = l \ln \frac{F}{F_{th}}, \tag{3}$$

where D is the ablation depth, l is a characteristic depth, and F and F_{th} are the incident and threshold fluences, respectively. F_{th} value is taken from the experimental data, and l is an adjustable parameter. At low laser fluences ($<1\,\mathrm{J\,cm^{-2}}$), equation (3) is in good agreement with the experimental results for $l = 22$ nm and $F_{th} = 0.12\,\mathrm{J\,cm^{-2}}$. Here, l has almost the same value as the optical penetration depth defined by the absorption coefficient taken from the reference ($1/\alpha = 18$ nm). The increase in the laser fluence results in a sharp increase in the ablation depth. Equation (3) is also valid for the high-fluence region; however, a significant change in the parameter l is needed. In the range of fluences between 1 and $10\,\mathrm{J\,cm^{-2}}$, l should be assigned a value of 148 nm. This correction to the parameter l can be related to the contribution of the electron thermal diffusion to the process of energy redistribution and can be regarded as the average depth of electron diffusion.

Our simulations confirm this hypothesis only partially. Figure 4 represents the ablation rate in Fe as a function of the laser fluence for different conditions in what concerns energy dissipation by electron heat conduction. The black dots refer to the results obtained when the electron thermal diffusion is not taken into account, i.e. the absorption is defined by $1/\alpha$. As one can see, the change in the ablation rate and the second threshold for ablation exist even in this case. One should, therefore, deduce that the reason for the ablation rate increase at high laser fluences is not directly connected with the electron thermal diffusion.

The expansion dynamics and the ejection of the material are mainly governed by the pressure developed as a result of the heating of the material. Figure 5 presents the dependence of the maximal pressure developed in the absorbing volume on the applied laser fluence. The results are obtained for the case when the electron thermal diffusion is not taken into account. As one can see, the dependence of the pressure developed in the material on the laser fluence has a behaviour similar to the ablation depth.

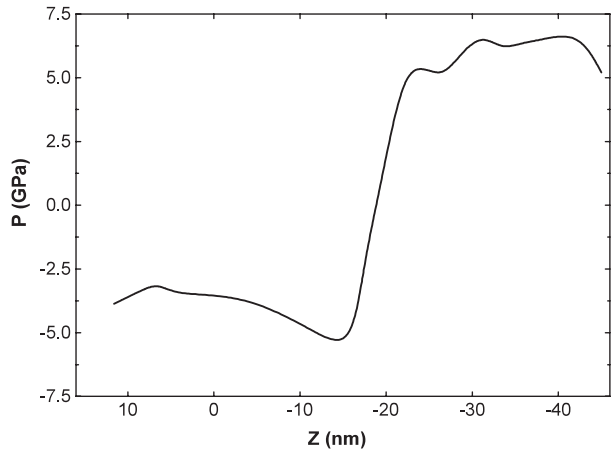

Figure 6. Depth distribution of the pressure developed in the material 20 ps after the laser pulse onset. Positive values represent compression, negative values, tension stress. $\tau_p = 0.1$ ps, $F = 0.15\,\mathrm{J\,cm^{-2}}$.

The steep rise in the pressure can be attributed to the introduction of different mechanisms of material removal. At fluences near the ablation threshold, the degree of overheating is not sufficient to cause fast transition of the heated material into a gas phase. Instead, the main part of the material is ejected in the form of big clusters. The fast heating of the material produces strong compression and tension waves that propagate into the material (figure 6). At a certain depth, the tension stress exceeds the strength of the material and causes fractures in the sample. As a result, a big portion of material can be ejected. This process, referred to as spallation, is observed also in organic solids [16] and MD simulations of Lennard-Jones solids [15]. With the increase in laser fluence, significant overheating of the absorbing volume takes place. The main part of the material is quickly transformed into overheated liquid, which decomposes into gas and liquid droplets (phase explosion) several picoseconds later. At fluences of the order of several hundreds of $\mathrm{mJ\,cm^{-2}}$, the temperature in the material starts to exceed the critical one. Above this temperature, the main part of the absorbing material is rapidly decomposed into the gas phase. This process is

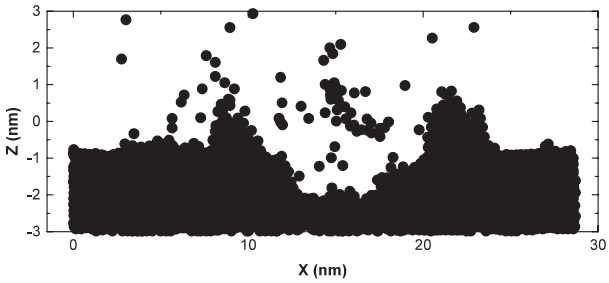

Figure 7. Snapshot of the atomic configuration taken 50 ps after the laser pulse onset. $\tau_p = 0.1$ ps, $F = 2\,\mathrm{J\,cm^{-2}}$. The molten material has solidified around the hole, forming a recast layer.

accompanied by a steep rise in the pressure developed in the material and results in a higher ablation rate.

However, as one can see in figure 4, the dependence of the ablation depth related only to this mechanism gives a lower value for the fluence where the ablation rate changes (second ablation threshold) and also an ablation rate differing from the experimental data.

In general, the processes described earlier take place also in the case when electron thermal diffusion is taken into account. The inclusion of the electron heat conduction in the process is related to an increase in the effective depth of energy penetration. On the one hand, this leads to overheating of a larger volume of material. On the otherhand, however, it is also connected with an increase in the heat losses in the material and to a decrease in the degree of overheating. As a result, the second ablation threshold fluence shifts to a higher value and the ablation rate increases. The increase in the heat losses is also related to the formation of a significant amount of molten phase which can be expelled by the strong recoil pressure developed at high fluences. This is another mechanism of increasing the ablation depth. The ejected molten material solidifies, forming a recast layer around the hole (figure 7).

Based on the above-mentioned results, one could draw the following conclusion: the presence of a second, higher, ablation rate at laser fluences above several hundreds of $\mathrm{mJ\,cm^{-2}}$ has to do with the fast overheating of the absorbing volume at temperatures above the critical one and with a steep rise in the pressure developed in the material. In addition, the dissipation of the energy more deeply into the material as compared with the optical penetration depth $(1/\alpha)$ due to the electron heat diffusion affects the ablation depth. Thus, using equation (3) at high laser fluences yields an overestimation of the average depth of electron diffusion. As one can see in figure 4, when one uses for the electron heat diffusion length the value $l = 148$ nm (taken on the basis of equation (3) and the experimental data in figure 3, for fluences ranging from 1 to $10\,\mathrm{J\,cm^{-2}}$), the simulation produces values for the ablation depth significantly higher than indicated by the experimental data. The estimation of the electron heat diffusion length using equation (2) gives an average value of about 100 nm for fluences in the range 1–$10\,\mathrm{J\,cm^{-2}}$. With this value, the simulation results are in acceptable agreement with the experimental data (figure 8).

The decrease observed in the ablation rate with the rise in the pulse duration can be attributed to the contribution of the heat diffusion losses. Figure 9 shows the evolution of

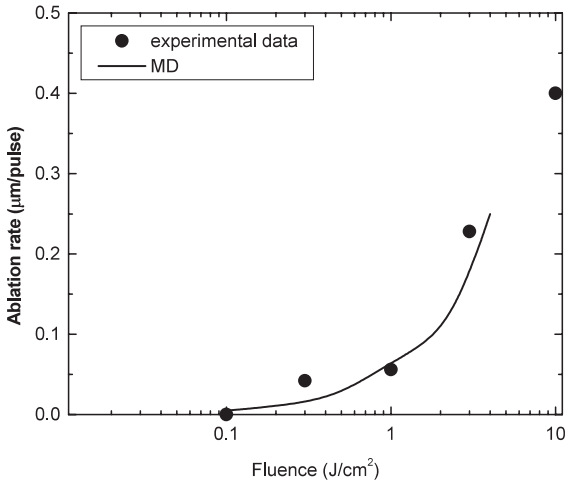

Figure 8. Ablation rate in Fe as a function of the laser fluence at $\tau_p = 0.1$ ps.

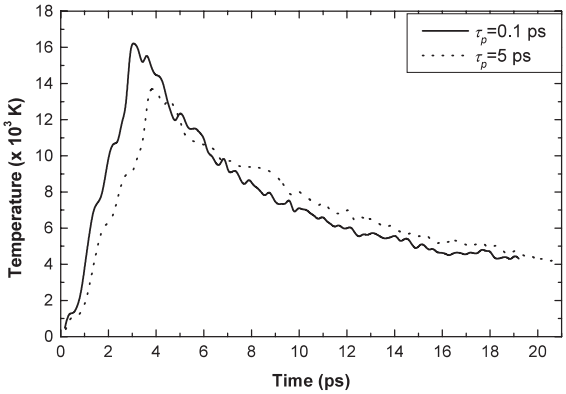

Figure 9. Evolution of the average temperature in the absorbing volume at $\tau_p = 0.1$ ps and 5 ps, $F = 2\,\mathrm{J\,cm^{-2}}$.

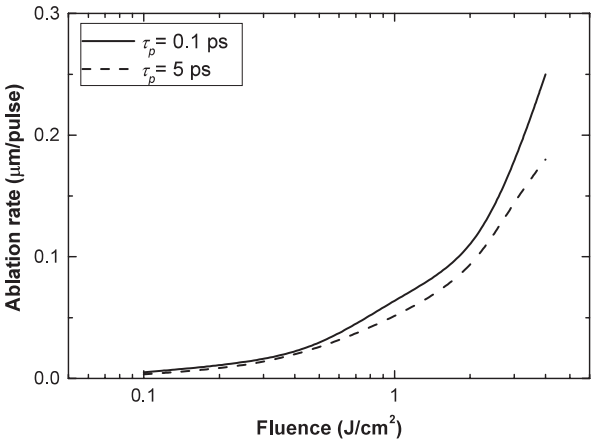

Figure 10. Ablation rate in Fe as a function of the laser fluence.

the average temperature in the absorbing volume for the cases of $\tau_p = 0.1$ and 5 ps and $F = 2\,\mathrm{J\,cm^{-2}}$. As one can see, the increase in τ_p results in a decrease in both the degree of overheating and the temperature gradients of heating. This leads to a drop in the ablation rate (figure 10). Furthermore, due to the lower temperature of the molten material in the hole, it has a higher viscosity compared with the femtosecond

regime. As a result, melt expulsion by the recoil pressure is hindered, and a significant part of the melt remains in the crater.

5. Conclusions

In the analysis of ablation of Fe with ultrashort laser pulses, we applied MD simulations to reveal the mechanisms involved in the process. The results clearly show the existence of two different modes of ablation, namely, at low ($<1\,\mathrm{J\,cm^{-2}}$) and at higher laser fluences. At fluences of about several $\mathrm{mJ\,cm^{-1}}$, the overheating of the material above the critical temperature leads to a sharp rise in pressure in the volume, which, in turn, causes an increase in the ablation rate. In addition, due to the electron heat diffusion, the overheating encompasses a larger volume of material. An increase in the pulse duration brings about a significant rise in the heat losses, so that a lower smaller ablation rate is observed. The process of energy dissipation caused by the electron heat diffusion is accompanied by the formation of a molten phase, which plays an important role in the ablation process.

Acknowledgments

This work is supported by the BMBF under Project No 13N7710/6 (PRIMUS), Germany, and by the Bulgarian National Science Foundation under contract F-1209.

References

[1] Chichkov B N, Momma C, Nolte S, von Alvensleben F and Tünnermann A 1996 *Appl. Phys.* A **63** 109
[2] Preuss S, Demchuk A and Stuke M 1995 *Appl. Phys.* A **61** 33
[3] Zhu X, Naumov A Yu, Villeneuve D M and Corkum P B 1999 *Appl. Phys.* A **69** S367
[4] Shirk M D and Molian P A 1998 *J. Laser Appl.* **10** 1
[5] Nolte S, Momma C, Jacobs H, Tünnermann A, Chichkov B N, Wellegehausen B and Welling H 1997 *J. Opt. Soc.* B **14** 2716
[6] Wellershoff S S, Hohlfeld J, Güdde J and Matthias E 1999 *Appl. Phys.* A **69** S99
[7] Furusawa K, Takahashi K, Kumagai H, Midorikawa K and Obara M 1999 *Appl. Phys.* A **69** S359
[8] Zhigilei L V 2003 *Appl. Phys.* A **76** 339
[9] Banks P S, Feit M D, Rubenchik A M, Stuart B C and Perry M D 1999 *Appl. Phys.* A **69** 377
[10] Wynne A E and Stuart B C 2003 *Appl. Phys.* A **76** 373
[11] Klein-Wiele J-H, Marowsky G and Simon P 1999 *Appl. Phys.* A **69** S187
[12] Nishikawa H, Kanai M, Szabo G and Kawai T 2000 *Phys. Rev.* B **61** 967
[13] Bonse J, Baudach S, Kautek J and Lenzner M 2002 *Appl. Phys.* A **74** 19
[14] Gamaly E G, Rode A V, Tikhonchuk V T and Luther-Davies B 2002 *Appl. Surf. Sci.* **8094** 1
[15] Perez D and Lewis L 2003 *Phys. Rev.* B **67** 184102
[16] Schäfer C, Urbassek H M and Zhigilei L V 2002 *Phys. Rev.* B **66** 115404
[17] Anisimov S I, Inogamov N A, Oparin A M, Rethfeld B, Yabe T, Ogawa M and Fortov V E 1999 *Appl. Phys.* A **69** 617
[18] Allen M P and Tildesley D J 1987 *Computer Simulation of Liquids* (Oxford: Clarendon)
[19] Girifalco I A and Weizer V G 1959 *Phys. Rev.* **114** 687
[20] Kanavin A P, Smetanin I V, Isakov V A, Afanasiev Yu V, Chichkov B N, Wellegehausen B, Nolte S, Momma C and Tünnermann A 1998 *Phys. Rev.* B **57** 14698
[21] Lynch D W and Hunter W R 1985 *Handbook of Optical Constants of Solids* ed E D Palik (New York: Academic)
[22] Grigorev I S and Mejlikhov E Z 1991 *Fizicheskie Velichini* Energoatomizdat